ASDA FEA ASSIGNMENT 2024-25

Table of Contents

Table of Figures 1
Table of Tables 2
1. Objective of the Analysis 3
2. Definition of Geometry, Loading Conditions, and Constraints 3
2.1 Geometry 3
2.2 Material Properties 4
2.3 Loading Conditions 4
2.4 Constraints 4
3. Details of the FE Model 5
3.1 Element type Selection 5
3.1.1 Justification 5
3.2 Geometry 5
3.3 Meshing 6
3.4 Boundary Conditions 6
4. Results 7
4.1 Analysis Part 1 7
1.1.1 Theoretical values 7
4.1.2 Ansys APDL values 7
4.2 Analysis Part 2 - Torsional Rotation 8
4.2.1 Theoretical values 8
4.2.2 Ansys APDL values 8
4.3 Comparison of Theoretical and FEA Displacements: 9
4.4 Part III 10
4.4.1 Ansys APDL values 10
4.4.2 Analysis 11
5. Derivation of Equation (6): Twist Angle in Single-Cell Thin-Walled Structures Under Torsion 13
Step 1: Shear Flow and Torque 13
Step 2: Shear Stress 13
Step 3: Twist Angle via Strain Energy 13
Step 4: Torsional Constant 14
Final Formulation 14
Key Assumptions and Insights 4
6. Concluding Remarks 14

Table of Figures

Figure 1- Starboard Wing Planform 3
Figure 2- Cross section of the Wing (The bold rectangular shape) 3
Figure 3- Common Cross Section of Wind Spar in Ansys APDL 6
Figure 4- An Oblique View of the Model 6
Figure 5- The Uniform Edge Element 6

Figure 6- The Wing Spar Constrained At The Root 6
Figure 7- Deformed Beam From a Point Load Force 8
Figure 8- Deformed Beam From Torque Force 9
Figure 9 - Deformed Shape and von Mises Stress Distribution of Distributed Load 11

Table of Tables

Table 1- Aerodynamic Load Distribution 4
Table 2- Keypoint Positions In Active CS 5
Table 3- Aerodynamic Load Distribution 10
Table 4 - Values of Displacement and Rotation for 3rd Analysis 12

1. Objective of the Analysis

The purpose of this analysis is to evaluate the structural performance of a UAV's wing spar under defined conditions, where a common cross-section of the spar is a hollow rectangular shape (which can be seen in Figure 2). This analysis will be conducted by comparing an FEA analysis in Ansys APDL with theoretical calculations to validate the accuracy of the model.
The defined conditions are:

- "A point load of 1000.0 N in the z-direction applied at the centroid of the spar at station x= 2.0 m."
- "A concentrated torsional moment of 30.0 Nm applied at x = 2.0 m."

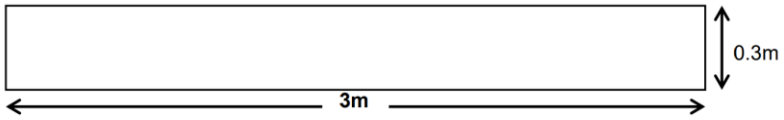

Figure 1- Starboard Wing Planform

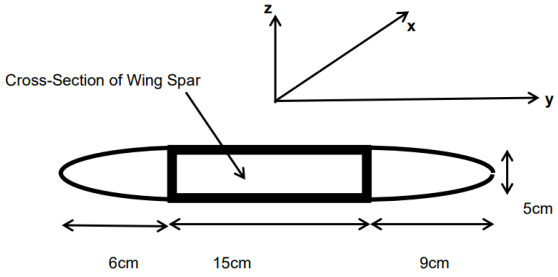

Figure 2- Cross section of the Wing (The bold rectangular shape)

This sort of analysis is not only relevant in testing a student's knowledge but is a practice seen many times in industry to test wing spars before prototype development. This process cuts down on the necessity for expensive physical prototypes and guarantees adherence to regulatory standards prior to testing in actual flight conditions.

2. Definition of Geometry, Loading Conditions, and Constraints

2.1 Geometry

The wing being analysed is a rectangular wing with a high aspect ratio and a hollow rectangular spar. The external dimensions of the spar are 15 cm wide, 5 cm tall, and 0.3 cm thick. The spar consists of an alloy of aluminium. It has a density of 2800 kg/m³. Its Young's modulus is 90 GPa. Its Poisson ratio is 0.28. Its yield strength is 300 MPa. Its ultimate tensile strength is 340 MPa. The UAV fuselage has a fully integrated attachment at the wing root.

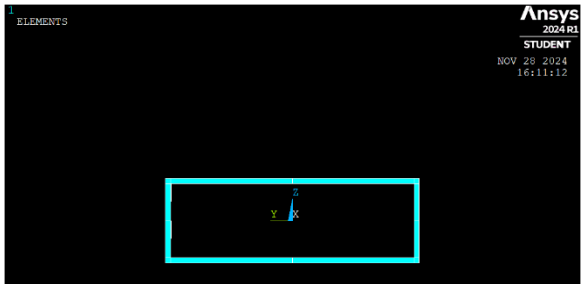

Figure 3- Cross Section of Wing Spar in Ansys APDL

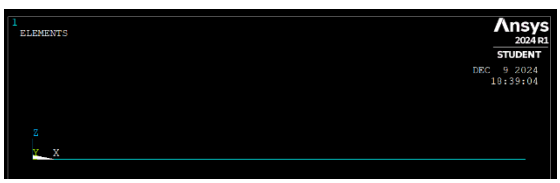

Figure 4- Side View of Wing Spar in Ansys APDL

2.2 Material Properties

The aluminium alloy used for the spar has the following properties:

- Density: 2800 kg/m³
- Young's Modulus: 90 GPa
- Poisson's Ratio: 0.28
- Yield Strength: 300 MPa
- Ultimate Tensile Strength: 340 MPa

Key Assumptions and Insights

1. **Thin-Walled Approximation**: Shear stress is uniformly distributed across the wall thickness.
2. **Single-Cell Assumption**: The structure encloses a single area A_m.
3. **Material Behavior**: Linear elastic behaviour is assumed for the material (shear modulus G).

2.3 Loading Conditions

For this assignment
The defined conditions are:

- Point Load: A point load of 1000.0 N in the z-direction applied at the centroid of the spar at station x= 2.0 m.
- Torsional Moment: A concentrated torsional moment of 30.0 Nm applied at x = 2.0 m.
- Aerodynamic Load Distribution: A distributed load in the z-direction applied at the following positions at the quarter chord position aft of the leading edge.

Table 1- Aerodynamic Load Distribution

Spanwise Location (x)	Load (N)
0.5m	485
1.0m	464
1.5m	426
2.0m	366
2.5m	260

2.4 Constraints

The wing is represented in the model as having a fully fixed support at the root, with all its translational and rotational degrees of freedom constrained. This is necessary to model the attachment to the fuselage and to predict the stress and displacement distribution along the span of the wing accurately.

Figure 5- Constrained Beam Model Representing the Wing Spar

3. Details of the FE Model

This section lists the methodology used to conduct the analysis in Ansys APDL.

3.1 Element Type Selection

In this analysis, the wing spar was modelled using a 2-node BEAM188 element type in ANSYS APDL
There are two nodes in this element, located at each end of the beam segment which makes it suitable for this analysis
Each node has six degrees of freedom (DOF):

- **Translational DOF**: UX, UY, UZ
- **Rotational DOF**: ROTX, ROTY, ROTZ

These degrees of freedom allow the element to capture accurately the effects of bending, axial deformation, twisting, and shearing—essential for structural behaviour analysis of the wing spar.

3.1.1 Justification

Geometry and Loading Requirements

The spar for the wing spans 3 meters, and for that, we used a beam element called Beam188 2-node element. A 2-node straight beam element is ideal for this structure and loading condition, giving linear interpolation of displacements and rotations. Beam189, a higher-order 3-node element, would have been overkill for such a simple model.

Computational Efficiency

Beam188 is simply less computationally heavy than other elements such as Beam189. It uses fewer nodes and captures bending and torsional effects just as well, if not better, than Beam189, whose additional node in each element would make it require too many resources and deliver solutions much less quickly than would be feasible in a timed context. In short, Beam188 is the more efficient element.

Accuracy of Results

Even though the 2-node element type is less accurate than the 3-node element type, under the given specified loads, deflection, slope, and torsion are reliably captured by the 2-node Beam188. Yet, the geometry is straight, and the loading conditions are simple. For these elementary situations, the added accuracy of quadratic interpolation found in Beam189 is not needed.

3.2 Geometry

The wing spar is modelled as a line with 2 key points (Figure 3) using an element type of 2 node188 and was constructed using a common cross-section of a hollow rectangle (Figure 4) with the following position:

Table 2- Keypoint Positions In Active CS

Key point 1 in active CS

x	y	z
0	0	0

Key point 2 in active CS

x	y	z
3	0	0

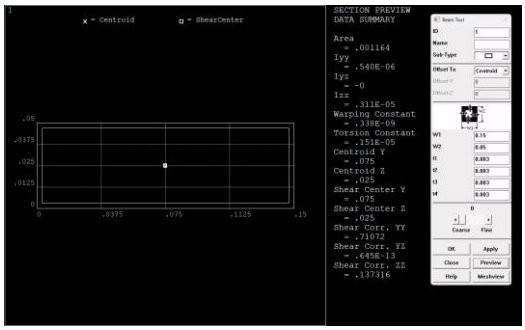

Figure 6- Common Cross Section of Wind Spar in Ansys APDL

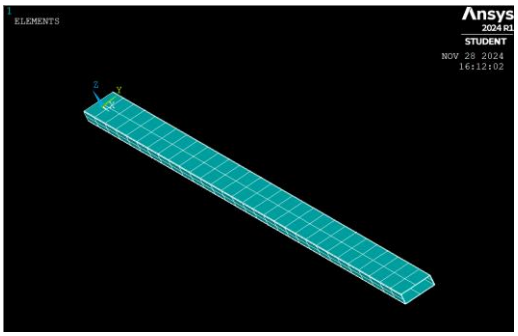

Figure 7- An Oblique View of the Model

3.3 Meshing

The beam was divided into 30 elements along the length of the beam. Each element has a uniform edge length of 0.1 meters. The mesh density also ensure that the load points coincide with the node locations. This balances between computational resources and having an accurate enough solution. All the points where the load is applied are at the same places as the nodes in the mesh.

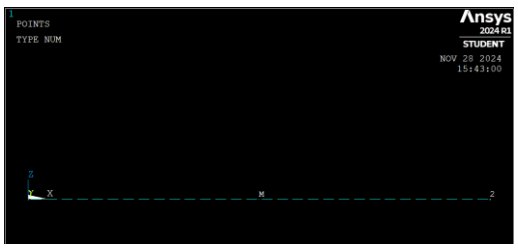

Figure 8- The Uniform Edge Element

3.4 Boundary Conditions

The wing is represented in the model as having a fully fixed support at the root, with all its translational and rotational degrees of freedom constrained. This is necessary to model the attachment to the fuselage and to predict the stress and displacement distribution along the span of the wing accurately.

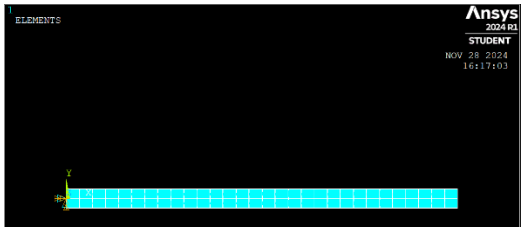

Figure 9- The Wing Spar Constrained At The Root

4. Results

In this section, the theoretical calculations are given for the deflection under a point load and the torsional rotation of the UAV wing spar.

4.1 Analysis Part 1

1.1.1 Theoretical values

Calculation of Second Moment of Area (I):

$$I = \frac{ab^3}{12} - \frac{(a-2t)(b-2t)^3}{12}$$

Where:

- $a = 0.15\,\text{m}$
- $b = 0.05\,\text{m}$
- $t = 0.003\,\text{m}$

Substituting the values:

$$I = \frac{0.15 \times (0.05)^3}{12} - \frac{(0.15 - 2 \times 0.003)(0.05 - 2 \times 0.003)^3}{12}$$

$$I = 5.40292 \times 10^{-7}\,\text{m}^4$$

Deflection under Point Load

The deflection z at the point of load for the beam is given by:

$$z = \frac{PL^3}{3EI}$$

Where:

- $P = 1000\,\text{N}$
- $L = 2\,\text{m}$
- $E = 90 \times 10^9\,\text{Pa}$
- $I = 5.40292 \times 10^{-7}\,\text{m}^4$

Substituting the values:

$$z = \frac{1000 \times (2)^3}{3 \times (90 \times 10^9) \times (5.40292 \times 10^{-7})}$$

$$z = 0.05484003\,\text{m}$$

4.1.2 Ansys APDL values

1. **Point Load**:
 - **Location**: Centroid of the spar at station x = 2.0 m.
 - **Direction**: 1000 N in the z-direction.

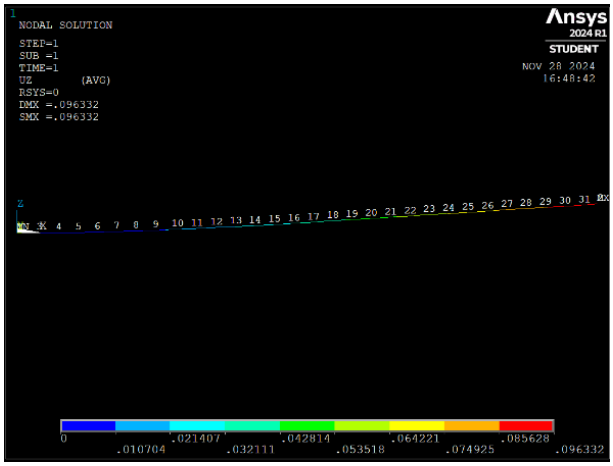

Figure 10- Deformed Beam From a Point Load Force

Node	UZ(m)
22	0.55202E-001

4.2 Analysis Part 2 - Torsional Rotation

4.2.1 Theoretical values

The torsional rotation θ is given by:

$$\theta = \frac{TL}{GK}$$

But first, we need to find Young Modulus G:

$$G = \frac{E}{2(1+v)}$$

Where:

- Possions ration $v = 0.28$
- Young Modulus $E = 90 \times 10^9$ Pa

$$G = 35156250000\ \text{Pa}$$

Then we find the only other unknown term (K):

$$K = \frac{2t^2(a-t)^2(b-t)^2}{at + bt - 2t^2}$$

$$K = 1.47632E-06\ \text{m}^4$$

Finally Substituting it into the Torsional Rotation with an applied torque of 30 at the station x = 2:

$$\theta = \frac{TL}{GK}$$

$$\theta = 0.001156029\ \text{radians}$$

4.2.2 Ansys APDL values

1 Torsional Moment:
- Location: Centroid of the spar at station x = 2.0 m.
- Direction: 30 Nm.

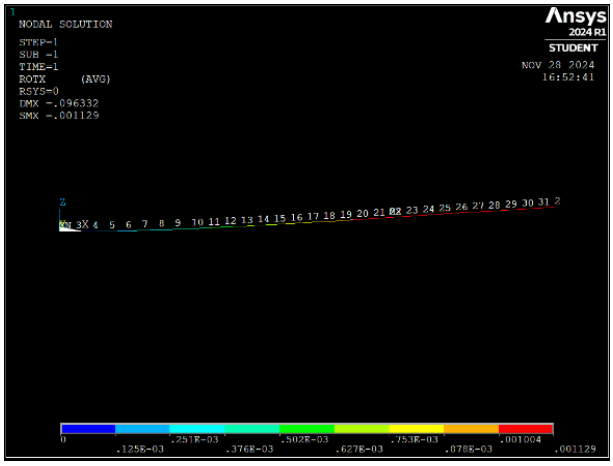

Figure 11- Deformed Beam From Torque Force

Node	ROTX
22	0.11294E-002

4.3 Comparison of Theoretical and FEA Displacements:

Analysis Part 1

We calculated the difference and the percentage difference to evaluate how well the theoretical and numerical results matched:

$$\text{Difference} = 0.055202\,\text{m} - 0.05484003\,\text{m} = 0.00036197\,\text{m}$$

$$\text{Percentage Difference} = \left(\frac{0.00036197}{0.05484003}\right) \times 100 \approx 0.66\%$$

This slight difference in percentage indicates that the theoretical model and the ANSYS simulation are highly correlated.

Analysis Part 2

The values obtained for the applied torsional moment that caused the rotational displacement were:

$$\text{Difference} = 0.001156029\,\text{radians} - 0.0011294\,\text{radians} = 0.000026629\,\text{radians}$$

$$\text{Percentage Difference} = \left(\frac{0.000026629}{0.001156029}\right) \times 100 \approx 2.3\%$$

The reason for this slightly larger difference between percentages when compared to Part 1 can be linked to the boundary conditions and FE discretization, to which rotational displacements are much more sensitive.

Possible Sources of Discrepancy

The results are nearly identical, but a few things could account for the minor discrepancies. First, the theoretical model could be making some overly simplified assumptions. For example, it might not have captured the precise nature of how the load is applied. Second, there could be differences in how the two models implement the boundary conditions. Third, the finite element method itself involves some inherent approximations that could lead to discrepancies if the two models aren't using the same number of elements for the same problem. Lastly, errors could have crept in via rounding.

Conclusion

The ANSYS results validate the theoretical model. The displacement values yield an acceptable engineering tolerance. The theoretical approach appears to be appropriate for this scenario. The models' consistent unit use and their minimal differences strongly suggest a right and tight simulation. Mesh density and material property "consistency," to use an ANSYS term, were also confirmed to be right and tight. All these factors strongly reinforce the validity of the ANSYS simulation.

4.4 Aerodynamic Load Distribution

Using ANSYS APDL software, we performed a finite element analysis to yield the ultimate tensile stress values. The yield criterion we used was the Von Mises, which combines all the individual stress components into a single equivalent value.

4.4.3 Model Setup

To offset the model a location offset was added to the common cross-section was added as seen in figure 9.

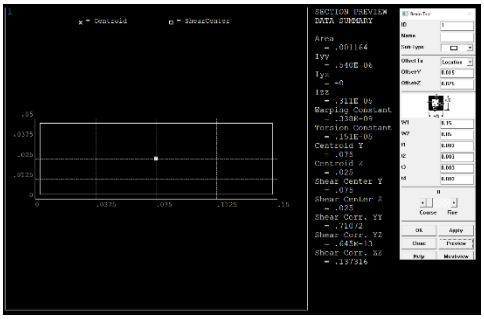

Figure 12- Common Cross Section Offset Menu

After which the beam was constrained, and forces were applied.

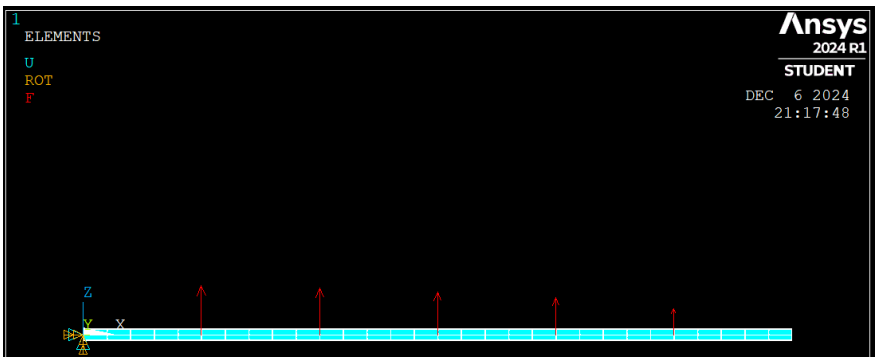

Figure 13- Aerodynamic Load Distribution Beam Setup

4.4.2 Ansys APDL values

- Aerodynamic Load Distribution: A distributed load in the z-direction applied at the following positions at the quarter chord position aft of the leading edge.

Table 3- Aerodynamic Load Distribution

Spanwise Location (x)	Load (N)
0.5m	485
1.0m	464
1.5m	426
2.0m	366
2.5m	260

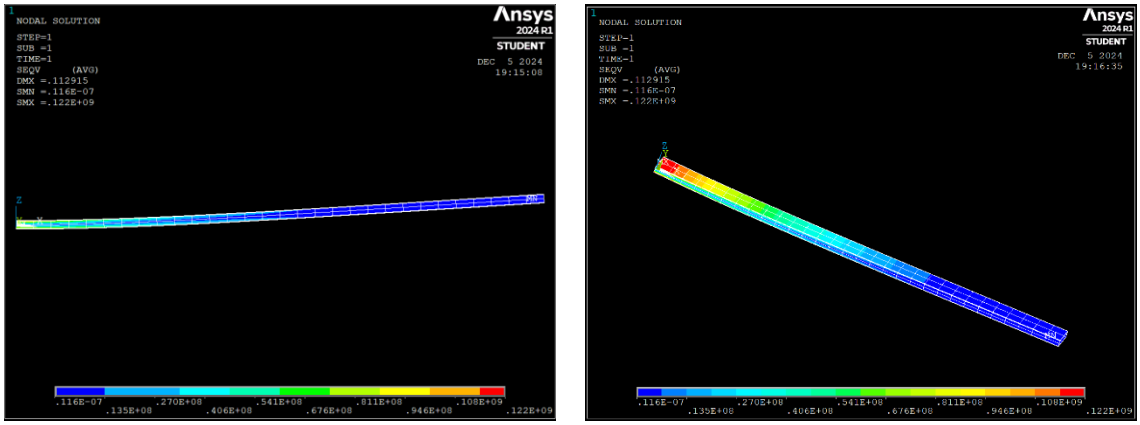

Figure 14 - Deformed Shape and von Mises Stress Distribution of Distributed Load

Max Tensile Stress	Lowest Tensile Stress
0.122E+09	0.116E-07

4.4.2 Analysis

Material Properties (Aluminum Alloy):

- Yield Strength, σ_{yield}: 300 MPa
- Ultimate Tensile Strength, $\sigma_{ultimate}$: 340 MPa

Finite Element Analysis (FEA) Results:

- Maximum Tensile Stress, σ_{FEA}: 122 MPa

Safety Factors:

- Proof Factor, η_p: 1.25
- Ultimate Factor, η_u: 1.50

Calculations

4. **Allowable Stress Based on Proof Factor:**
   The proof factor ensures the operational stress level remains below the yield threshold, thus preventing permanent deformation.

$$\sigma_{\text{allowable, proof}} = \frac{\sigma_{yield}}{\eta_p} = \frac{300\,\text{MPa}}{1.25} = 240\,\text{MPa}$$

2. **Allowable Stress Based on Ultimate Factor:**
   The ultimate factor ensures the service stress level remains below the ultimate tensile strength, thereby preventing catastrophic failure.

$$\sigma_{\text{allowable, ultimate}} = \frac{\sigma_{ultimate}}{\eta_u} = \frac{340\,\text{MPa}}{1.50} \approx 226.67\,\text{MPa}$$

Comparing FEA Results with Allowable Stresses

- FEA Maximum Stress**:** $\sigma_{FEA} = 122\,\text{MPa}$

Verification Against Allowable Limits:

- Proof Factor Check: $122\,\text{MPa} < 240\,\text{MPa}$

- Ultimate Factor Check: $122\,\text{MPa} < 226.67\,\text{MPa}$

The FEA results show that the highest tensile stress in the UAV wing structure is 122 MPa. This value is much lower than the yield strength limit (240 MPa) and the ultimate strength limit (226.67 MPa) that we can use safely.

Implications:

- **Safety Margin:** The big difference between the real stress in the FEA and the stress allowed by the material means there is a strong safety margin. This safety margin acts like a shield, making sure the UAV wing can handle the loads it faces in real operations. We can say it does this without the wing bending or breaking.

- **Material Utilization:** The current design is clearly conservative, so there's lots of room to optimize it. Future designs could think about moving away from the materials we've used so far and reducing weight. This would help us use the materials we have in our structures more efficiently. This works by making the important parts of our designs stronger and better at carrying loads.

When a UAV wing structure bends under a load, the main internal stresses that develop are tension and compression. The side of the wing that is stretched gets tensile stress and the side that is pushed together gets compressive stress. Between these two areas is the "neutral axis," where the wing is neither stretched nor compressed. This is the point where the wing starts to switch from tensile to compressive stress. Understanding how the internal stresses are distributed in the wing structure is very important. This is because we need to make sure that both tensile stress and compressive stress don't go over the limits, we consider acceptable.

In summary, the analysis shows that the beam is firmly within the safety zone. It says that the beam handles both tension and compression well, and it does so mostly by staying under the material's yield strength. This means the beam stays elastic, which is very good for an efficient wing design.

ROT Y And Z displacement

The wing moves downwards from the root to the tip, reaching vertical displacements (U_Z) of about 0.108 m at the tip (in Table 4). At the same time, the wing rotates around the Y-axis (ROT_Y) to about -4.76×10^{-2} radians and around the X-axis (ROT_X) to about -2.57×10^{-3} radians. The negative values just come from the chosen coordinate system. They mean the wing twist and bend direction is opposite to the positive axes we defined. This is not a sign of any problems. The values we get from the experiment are all well within safe limits.

Table 4- Values of Displacement and Rotation for Aerodynamic Load Distribution

NODE	UX	UY	UZ	ROTX	ROTY	ROTZ
1	0.00E+00	0.00E+00	0.00E+00	0.00E+00	0.00E+00	0.00E+00
2	4.76E-04	-2.57E-05	1.13E-01	-2.57E-03	-4.76E-02	1.84E-16
3	5.40E-05	-1.88E-06	3.19E-04	-1.88E-04	-5.40E-03	2.93E-18
4	1.04E-04	-3.77E-06	1.16E-03	-3.77E-04	-1.04E-02	5.50E-18
5	1.50E-04	-5.65E-06	2.48E-03	-5.65E-04	-1.50E-02	7.13E-18
6	1.91E-04	-7.53E-06	4.23E-03	-7.53E-04	-1.91E-02	8.21E-18
7	2.29E-04	-9.42E-06	6.38E-03	-9.42E-04	-2.29E-02	9.34E-18
8	2.63E-04	-1.08E-05	8.88E-03	-1.08E-03	-2.63E-02	1.12E-17
9	2.94E-04	-1.23E-05	1.17E-02	-1.23E-03	-2.94E-02	1.31E-17
10	3.22E-04	-1.37E-05	1.48E-02	-1.37E-03	-3.22E-02	1.61E-17
11	3.46E-04	-1.51E-05	1.82E-02	-1.51E-03	-3.46E-02	1.59E-17
12	3.68E-04	-1.66E-05	2.18E-02	-1.66E-03	-3.68E-02	1.66E-17
13	3.86E-04	-1.75E-05	2.56E-02	-1.75E-03	-3.86E-02	1.88E-17
14	4.03E-04	-1.85E-05	2.96E-02	-1.85E-03	-4.03E-02	2.13E-17
15	4.18E-04	-1.95E-05	3.37E-02	-1.95E-03	-4.18E-02	2.36E-17

16	4.30E-04	-2.05E-05	3.80E-02	-2.05E-03	-4.30E-02	3.31E-17
17	4.40E-04	-2.15E-05	4.23E-02	-2.15E-03	-4.40E-02	4.43E-17
18	4.49E-04	-2.21E-05	4.68E-02	-2.21E-03	-4.49E-02	5.64E-17
19	4.56E-04	-2.27E-05	5.13E-02	-2.27E-03	-4.56E-02	6.84E-17
20	4.62E-04	-2.33E-05	5.59E-02	-2.33E-03	-4.62E-02	8.36E-17
21	4.66E-04	-2.39E-05	6.06E-02	-2.39E-03	-4.66E-02	1.05E-16
22	4.70E-04	-2.44E-05	6.53E-02	-2.44E-03	-4.70E-02	1.23E-16
23	4.72E-04	-2.47E-05	7.00E-02	-2.47E-03	-4.72E-02	1.37E-16
24	4.74E-04	-2.49E-05	7.47E-02	-2.49E-03	-4.74E-02	1.46E-16
25	4.75E-04	-2.52E-05	7.95E-02	-2.52E-03	-4.75E-02	1.52E-16
26	4.76E-04	-2.54E-05	8.43E-02	-2.54E-03	-4.76E-02	1.60E-16
27	4.76E-04	-2.57E-05	8.90E-02	-2.57E-03	-4.76E-02	1.69E-16
28	4.76E-04	-2.57E-05	9.38E-02	-2.57E-03	-4.76E-02	1.74E-16
29	4.76E-04	-2.57E-05	9.86E-02	-2.57E-03	-4.76E-02	1.81E-16
30	4.76E-04	-2.57E-05	1.03E-01	-2.57E-03	-4.76E-02	1.85E-16
31	4.76E-04	-2.57E-05	1.08E-01	-2.57E-03	-4.76E-02	1.84E-16

5.Derivation of Equation (6): Twist Angle in Single-Cell Thin-Walled Structures Under Torsion

We derive the twist angle θ for a single-cell thin-walled structure under torsion, starting from the general principles outlined in ASDA 1.

Step 1: Shear Flow and Torque

The relationship between torque T and shear flow q is given by:

$$T = 2A_m q$$

where:

- T: Applied torque
- A_m: Area enclosed by the midline of the thin-walled cross-section
- q: Shear flow.

From this, the shear flow q is expressed as:

$$q = \frac{T}{2A_m}$$

Step 2: Shear Stress

The shear stress τ is related to the shear flow by the wall thickness t:

$$\tau = \frac{q}{t}$$

Step 3: Twist Angle via Strain Energy

Using the strain energy approach for torsion, the twist angle per unit length is derived as:

$$\frac{d\theta}{dz} = \frac{q}{Gt}$$

where G is the shear modulus. Integrating over the length L, the total twist angle is:

$$\theta = \int_0^L \frac{q}{Gt} dz$$

For a constant wall thickness t, this simplifies to:

$$\theta = \frac{T}{2A_m G} \oint_s \frac{ds}{t}$$

Step 4: Torsional Constant

The torsional constant K is introduced as:

$$K = 4A_m^2 \left(\oint_s \frac{ds}{t} \right)^{-1}$$

This simplifies the twist angle expression to:

$$\theta = \frac{TL}{GK}$$

Final Formulation

Combining the above, the twist angle θ is derived as:

$$\theta = \frac{TL}{4A_m^2 G} \oint_s \frac{ds}{t} = \frac{TL}{GK}$$

This confirms the derivation of Equation (6), connecting the applied torque T, structural geometry, and material properties.

6. Concluding Remarks

The structural soundness of the UAV wing spar was assessed and found satisfactory. The spar was evaluated using both theoretical calculations and finite element analysis (FEA) in ANSYS APDL. Correlation between the two methods was excellent, with results that are within an acceptable range for engineering tolerances. A comparison of the displacement results and the angular rotation (which is not a displacement in the usual sense but certainly is a kind of deformation) confirmed the study author's total understanding of their finite element method, along with its function and purpose. The FEA results were also zeroed in on in order to evaluate the spar structure in more detail.

Structural Integrity Assessment

The tensile and compressive stresses in the spar, derived from the analysis, are below the yield strength. Using a proof factor of 1.25 and an ultimate factor of 1.5, the safety for bending and twisting has been confirmed and is well above any reasonably expected standard.

$$\sigma_{\text{allowable, ultimate}} = \frac{\sigma_{ultimate}}{\eta_u} = \frac{340\ \text{MPa}}{1.50} \approx 226.67\ \text{MPa} \qquad \sigma_{\text{allowable, proof}} = \frac{\sigma_{yield}}{\eta_p} = \frac{300\ \text{MPa}}{1.25} = 240\ \text{MPa}$$

Non-Strength Considerations

The angular deformation was found to be minimal, which means that our aerodynamic performance is as we expect it to be under operational conditions. Still, we should look closely at the small changes in incidence since they could affect our lift distribution.

Final Remarks

This research confirms that using beam elements (BEAM188) can produce accurate structural analyses of wing spars in unmanned aerial vehicles, or UAVs. This type of element is necessary to achieve a balance between computational efficiency and accuracy. The main structural element of the UAV wing, the wing spar, was analysed under conditions that closely simulate what the wing would experience in flight. The analysis results indicate that the wing spar does in fact meet all relevant structural and safety requirements.